Nonenzymatic Sensor for Hydrogen Peroxide using a Carbon Paste Electrode Modified with a Composite Consisting of Silver Nanoparticles, poly(*o*-aminobenzoic acid) and Magnetite

Sanoe Chairam[1,], Wongduan Sroysee[1], Chantanee Boonchit[1], Chayanee Kaewprom[1], Tivagorn Goedsak Na Wangnoi[1], Maliwan Amatatongchai[1], Purim Jarujamrus[1], Suparb Tamaung[1] and Ekasith Somsook[2]*

[1] Department of Chemistry and Center of Excellence for Innovation in Chemistry, Faculty of Science, Ubon Ratchathani University, Warin Chamrap, Ubon Ratchathani 34190, Thailand.
[2] NANOCAST Laboratory, Center for Catalysis, Department of Chemistry and Center of Excellence for Innovation in Chemistry, Faculty of Science, Mahidol University, 272 Rama VI Rd. Rachathewi, Bangkok 10400, Thailand.
*E-mail: sanoe.c@ubu.ac.th

A nonenzymatic hydrogen peroxide (H_2O_2) sensor using a carbon paste electrode (CPE) modified with a composite consisting of silver nanoparticles (AgNPs), poly(*o*-aminobenzoic acid) (P(ABA)) and magnetite (Fe_3O_4) is reported. The AgNPs-P(ABA)-Fe_3O_4 composite was prepared under sonication and characterized using transmission electron microscopy (TEM), thermogravimetric analysis (TGA), and vibrating sample magnetometer (VSM). Electrochemical investigations indicated that a carbon paste electrode modified with AgNPs-P(ABA)-Fe_3O_4 exhibits excellent performance in the electrochemical reduction of H_2O_2 at an applied potential of -0.4 V versus Ag/AgCl (sat. 3.0 M KCl) in phosphate buffer solution. Under optimum condition, the calibration curve for H_2O_2 was obtained in a wide range of 5 µM to 5.5 mM with the limit of detection (LOD) of 1.74 µM (S/N = 3). The AgNPs-P(ABA)-Fe_3O_4 modified electrode has a good stability in practical conditions. In addition, the fabricated sensor was applied to determine H_2O_2 in real samples with good results.

1. INTRODUCTION

Modified electrodes containing either chemically reactive species or biomolecules have been widely used for the selective and sensitive determination of analytical targets [1]. Since hydrogen

peroxide (H_2O_2) is extensively employed in a variety of industries, including pharmaceutical, clinical, environmental and industrial applications, there are many analytical approaches for the determination of H_2O_2, such as titrimetry [2], spectrophotometry [3], fluorimetry [4], chemiluminesence [5], and electrochemistry [6-8]. Among several analytical techniques, electrochemistry has advantages over other methods, due to an easy-to-made, cost-effective, highly sensitive, and selective approach and its suitability for real-time detection.

The development of transducers including their bulk or surface modification has attracted attention in literature about modern electroanalytical methods. Carbon paste electrodes (CPEs) are one of the most commonly used electrodes in electrochemical investigations [9]. Applications of CPE have impacted on almost all of the fields of science, including clinical diagnostics, food quality control, security and environmental analysis [10]. Thus, the development of a suitable CPE is an important stage in electroanalytical research processes [11].

The direct electrochemistry of redox active biomolecules such as horseradish peroxidase (HRP) [12], cytochrome *c* [13], catalase (CAT) [14, 15], myoglobin [16, 17] and hemoglobin (Hb) [18] has received extensive attention owing to the highly challenging task of immobilization at the electrode surface; however, high costs, restricted activity and storage time, limit their use in the analytical field. Considering these drawbacks, nonenzymatic sensors for H_2O_2 have become highly desirable for sensor research for both academic research and industrial purposes.

To develop nonenzymatic sensors for H_2O_2, current efforts have focused on discovering novel materials with high electrocatalytic activity on transducers. Compared with other materials, these composite materials have attracted considerable attention because of their chemical, physical, and electronic properties, which are different from those of bulk materials [19]. Moreover, the size, surface area, and shape of nanomaterials have been tailored by designing a novel sensing platform to enhance the electrochemical performance. Several nanomaterials have been used to develop nonenzymatic sensors for H_2O_2, such as metal nanoparticles (NPs), metal oxide NPs, metal hexacyanoferrates, carbon-based nanomaterials, and conducting electroactive polymers [20].

Metal NPs play an important role in various research areas due to their unique properties. Among several metal NPs, silver nanoparticles (AgNPs) provide enormous possibilities for improving the electrochemical performance because of their unique characteristics, such as their large surface-to-volume ratio, highest electrical conductivity and excellent electrocatalytic behavior [21]. Recently, Chen *et al.*[22] provided a review of electrochemical sensing of hydrogen peroxide using AgNPs and other metal NPs. They report that compared with other metals, AgNPs have been frequently employed to fabricate nonenzymatic sensors for H_2O_2 due to their excellent catalytic activity and electrical conductivity.

Conducting electroactive polymers are important materials in academic and industrial purposes because of their optical and electrical properties. Several conducting electroactive polymers containing polyenes or polyaromatics, such as polyacetylene, polypyrrole, polyaniline, polythiophene, and poly(*p*-phenylene) have been reported extensively [23]. These polymers are prepared by chemical or electrochemical oxidation of the corresponding monomers in various organic solvents and/or in aqueous media. Among these polymers, polyaniline (PANI) and its derivatives have many advantages over others, such as low cost, ease of synthesis, good environmental stability, high electrical

conductivity, and excellent redox recyclability [24, 25]. Because of their unique properties, they have been often employed as conducting fillers in the preparation of electrically conducting composites for the development of various electrochemical sensors [26].

Magnetic metal oxide nanoparticles (NPs), especially iron oxides, have been extensively employed in a variety of fields. At a diameter less than 20 nm, these NPs are often in a superparamagnetic state at room temperature, and are magnetic only in the presence of a magnetic field [27]. Owing to their unique magnetic properties, they are very useful for chemical, physical, biological, environmental and biomedical applications, such as a catalyst support, in magnetic separation, and so on [28]. Recently, Zhu and Diao [29] reported a review of synthesis, functionalization, and applications of magnetic NPs. Among several magnetic iron oxide NPs, magnetite (F_3O_4) has been usually employed to fabricate nonenzymatic sensors, due to their easy preparation, reproducibility of synthesis and various surface modifications by organic materials.

It has been previously reported that carboxylated macromolecules can be attached onto the surface of magnetite via carboxylic acid functional groups [30, 31]. In addition, AgNPs have a strong tendency to adsorb onto carboxylated macromolecules, due to the cationic selectivity of the negatively charged carboxylated groups [32, 33]. Thus, in this study, a composite consisting of silver nanoparticles (AgNPs), poly(*o*-aminobenzoic acid) (P(ABA)) and magnetite (Fe_3O_4) was prepared under sonication, and was casted onto a carbon paste electrode. The experimental parameters of AgNPs-P(ABA)-Fe_3O_4 modified electrode were investigated including loading solution of AgNPs-P(ABA)-Fe_3O_4 composite, pH of buffer solution and applied potential. To explore its potential application, a nonenzymatic sensor using a carbon paste electrode modified with AgNPs-P(ABA)-Fe_3O_4 composite was also employed to determine H_2O_2 in pharmaceutical products compared with a standard method.

2. MATERIALS AND METHODS

2.1 Apparatus and instruments

All electrochemical measurements were carried out using an eDAQ potentiostat (model EA161) equipped with a e-corder 210 and e-Chem v2.0.13 software. A conventional three-electrode system was used with a bare or modified MCPE as a working electrode, the Ag/AgCl (sat. 3.0 M KCl) as a reference electrode, and a platinum (Pt) wire as a counter electrode. A 713 pH meter (Metrohm) was used to monitor the pH of phosphate buffer. TEM images were recorded employing a JEOL JSM-2010 transmission electron microscope (TEM) by accelerating at a voltage of 200 kV. Samples for the TEM measurements were prepared by dispersing a drop of a sample solution on a Formvar-coated Cu grid. Thermal properties were measured using a TG8120 RIGAKU instrument analyzer. The thermal decomposition process was simultaneously recorded online using TA Instrument's Universal Analysis TP2 MeasFile software (version 1.30). 5-10 mg of sample were loaded into an alumina (Al_2O_3) crucible, and heated from 30 °C to 700 °C with an increase in in temperature at a rate of 10 °C min^{-1} under flowing nitrogen gas (N_2) at 20 cm^3 min^{-1}. The mass saturation magnetization (M_s) of the as-

prepared samples was performed by a Lakeshore Model 7404 vibrating sample magnetometer (VSM). The magnetic parameters of each sample at 298 K were determined from hysteresis loops produced by the VSM curve. The saturation magnetization was reached at an applied field of 10 kOe. The magnetization data as a function of the applied field were plotted.

2.2 Materials and solutions

All chemicals in this study were used as received without further purification. Iron (II) chloride tetrahydrate ($FeCl_2 \bullet 4H_2O$) and iron (III) chloride anhydrous ($FeCl_3$), ammonium persulfate $(NH_4)_2S_2O_8$, *o*-aminobenzoic acid (*o*-Aba) and graphite powder (20 μm) were purchased from Sigma-Aldrich. Sodium hydroxide (NaOH) was purchased from Carlo Erba. All aqueous solutions were freshly prepared using de-ionized (DI) water (resistance (R) ≥ 18.2 MΩ•cm) purified with a Nanopore ultrapure water system. All electrochemical measurements were carried out using phosphate buffer (0.1 M, pH 7.5) as a supporting-electrolyte solution. The phosphate buffer with various pH values was prepared by mixing appropriate volumes of 0.1 M NaH_2PO_4 and 0.1 M Na_2HPO_4 solutions and then adjusted to the desired pH with NaOH or H_3PO_4.

2.3 Preparation of AgNPs-P(ABA)-Fe₃O₄ nanocomposite

A poly(o-aminobenzoic acid) (P(ABA)) was prepared using chemical polymerization as reported by Chan *et al*.[34], while Fe_3O_4 NPs were prepared by the co-precipitation method as reported by Schwertmann and Cornell [35] with some modifications. According to the polymer-stabilized iron oxide NPs reported by Boyer *et al*.[31], a composite consisting of AgNPs, P(ABA) and Fe_3O_4 was prepared by the following procedure. Approximately 11.9 mg of Fe_3O_4 NPs and 12.2 mg of P(ABA) was sonically dispersed in 1.0 cm^3 of DI water for 30 min to form a homogeneous suspension. Then, 0.1 cm^3 of 0.3 M $AgNO_3$ was injected into the mixed solution and then sonicated for an additional 15 min. Subsequently, 15.6 mg of $NaBH_4$ dissolved in 1.0 cm^3 of DI water was added into the reaction solution, in order to reduce Ag^+ ions to AgNPs. The resulting composite was isolated magnetically and washed with DI water followed by ethanol, and finally dried in an oven at 40 °C for 6 h. The schematic illustration for preparation of AgNPs-P(ABA)-Fe_3O_4 nanocomposites is shown in Figure 1.
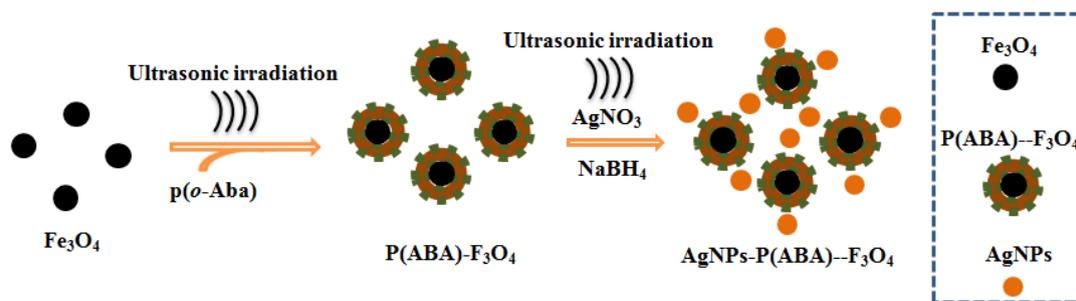

Figure1. Schematic illustration for preparation of AgNPs-P(ABA)-Fe₃O₄ nanocomposite.

2.4 Preparation of modified carbon paste electrodes

A magnetic carbon paste electrode (MCPE) was constructed following previously reported procedures [36, 37] with some modification as reported elsewhere. Briefly, 4 pieces of neodymium permanent magnet (2 mm diameter, 1.0 cm long) were inserted a cylindrical glass tube (3 mm diameter, 4.5 cm long). Then, graphite powder (100 mg) and mineral oil (30 μL) were hand-mixed in a mortar to form a homogeneous paste. Subsequently, a composite of graphite and mineral oil was packed into a cylindrical glass tube by pressing the end into the paste composite to a depth of approximately 3 mm. Then, a piece of copper wire (50 μm diameter, 12 cm long) was inserted into a cylindrical glass tube from the other end until the end of copper wire was buried into the graphite/mineral oil composite inside the glass tube. The electrical contact was established via a copper wire. Then, the flat surface of MCPE was manually smoothed using weighing paper and rinsed with DI water. Finally, the obtained electrode was allowed to harden at the ambient temperature and stored in a desiccator when not in use.

A carbon paste electrode modified with AgNPs-P(ABA)-Fe_3O_4) was fabricated by casting 20 μL of AgNPs-P(ABA)-Fe_3O_4 suspension (10 mg cm^{-3}) onto the electrode surface of the MCPE, and then air dried at the ambient temperature. The amount of composite loaded on the magnetic electrode can be varied by controlling the volume of the loading solution. The magnets inside the glass tube prevented spillage of the magnetic composite. In addition, Fe_3O_4, P(ABA)-Fe_3O_4 and AgNPs-Fe_3O_4 were loaded on the surface of the MCPE in the same procedures.
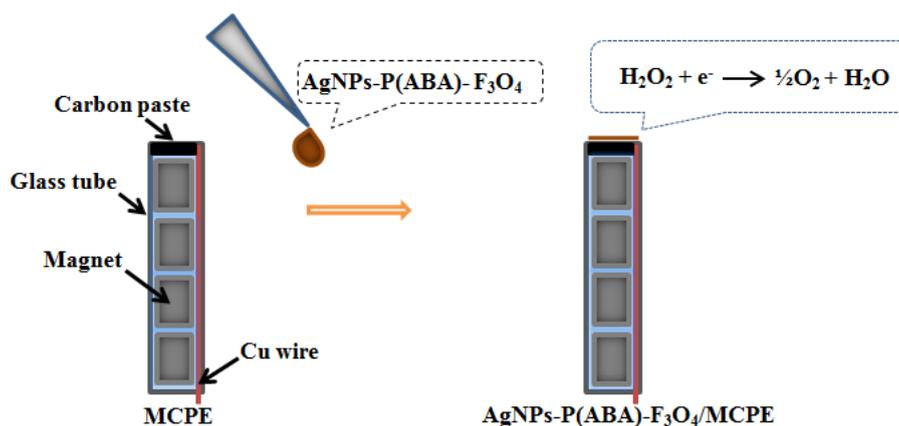
2.5 Electrochemical measurements

Figure 2. Schematic illustration for electrode modification and electrocatalytic process towards H_2O_2 sensing.

Cyclic voltammetric (CV) and amperometric experiments were performed in a thermostated electrochemical cell at 25 °C. Cyclic voltammograms of the Fe_3O_4, P(ABA)-Fe_3O_4, AgNPs-Fe_3O_4 and AgNPs-P(ABA)-Fe_3O_4 modified MCPE in the absence and presence of H_2O_2 in 0.1 M phosphate buffer (pH 7.5) were obtained by scanning a desired potential (versus Ag/AgCl, sat. 3.0 M KCl). The

supporting electrolyte solution was purged with highly pure N_2 for at least 10 min to remove O_2 and kept under N_2 atmosphere during the measurements. Amperometric experiments were carried out in a stirred batch system using a 10 cm^3 glass cell by applying a desired potential to the working electrode and adding freshly prepared aliquots of H_2O_2 standard solution. The schematic illustration for electrode modification and electrocatalytic process towards H_2O_2 sensing is shown in Figure 2.

2.6. Standard method for the determination of H_2O_2

To test the reproducibility and reliability of the developed sensor, H_2O_2 levels in two samples were determined three times with appropriate dilutions. To study the correlation of the present method with the standard method, the H_2O_2 values in real samples were measured using the $KMnO_4$ titrimetric standard method.

3. RESULTS AND DISCUSSION

3.1 Preparation of AgNPs-P(ABA)-Fe₃O₄ composite

According to previous reports [38, 39], the mechanisms for preparation of AgNPs-P(ABA)-Fe_3O_4 composite were described as follows. The magnetite NPs (Fe_3O_4) were prepared by the co-precipitation method from ferrous (Fe^{2+}) and ferric (Fe^{3+}) solutions with a stoichiometric molar ratio of 1:2 under an alkaline condition. The high density of hydroxyl groups on the surface of magnetic iron oxide NPs allows further chemical modification with carboxylic acid functional groups of P(ABA), yielding a P(ABA)-Fe_3O_4 composite. This technique leads to the fabrication of a nano-sized magnetic molecularly imprinted polymer (nano-MMIP) [40]. In the next step, AgNPs were synthesized from Ag^+ ions with the assistance of P(ABA)-Fe_3O_4 composite through the electrostatic interaction or chelation [41]. By prolonging the reaction time, the adsorbed Ag^+ ions were reduced to Ag^0 using $NaBH_4$ as a reducing agent, yielding a AgNPs-P(ABA)-Fe_3O_4 composite. Finally, the prepared magnetic composite easily collected using an external magnetic field without the additional centrifugation or filtration.

3.2 Characterization of AgNPs-P(ABA)-Fe₃O₄ composite

The morphology of the resulting products before and after modification was carried out by TEM measurements. Figure 3 shows representative TEM images of Fe_3O_4, P(ABA)-Fe_3O_4, AgNPs-Fe_3O_4 and AgNPs-P(ABA)-Fe_3O_4. It was found that the starting Fe_3O_4 mainly consisted of a nearly spherical shape with a diameter of 10-15 nm. The dark/light contrasts observed suggested a different phase composition in the resulting composites. The AgNPs were clearly found to be attached on the surface of magnetic support. Accordingly, it was concluded that the surface modification of Fe_3O_4 support was successful.
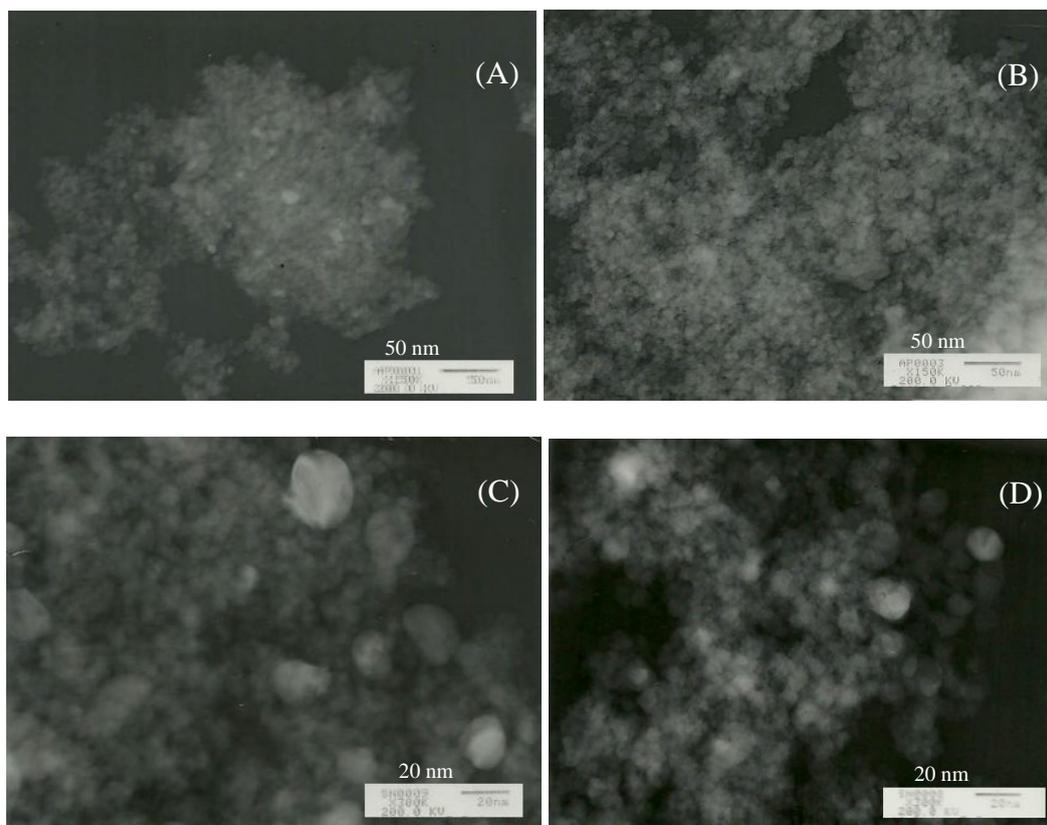
Figure 3. TEM images of (A) Fe$_3$O$_4$, (B) P(ABA)-Fe$_3$O$_4$, (C) AgNPs-Fe$_3$O$_4$, and (D) AgNPs-P(ABA)-Fe$_3$O$_4$. The scale bars (A-D) are 50, 50, 20 and 20 nm, respectively.

The thermal properties of the as-prepared samples were studies using thermogravimetric analysis (TGA). Figure 4A shows the TGA curves of Fe$_3$O$_4$, P(ABA), P(ABA)-Fe$_3$O$_4$ and AgNPs-P(ABA)-Fe$_3$O$_4$. Considering the organic component in samples, P(ABA) and P(ABA)-Fe$_3$O$_4$ lose weight easily upon heating. The TGA curve of P(ABA) shows three distinct stages of weight loss. The weight loss below 200 °C was due to physically absorbed water, and two major weight losses above 200 °C were attributed to the decomposition of the polymer chain [42]. The weight loss of P(ABA)-Fe$_3$O$_4$ was around 34.4 wt%, indicating the magnetite content about 65.6 wt% in P(ABA)-Fe$_3$O$_4$. The difference of weight losses between AgNPs-P(ABA)-Fe$_3$O$_4$ and P(ABA)-Fe$_3$O$_4$ was also attributed to the Ag content in AgNPs-P(ABA)-Fe$_3$O$_4$.

In order to investigate the magnetic properties of the as-prepared samples, VSM measurements were carried out at room temperature. Figure 4B shows the hysteresis loops of Fe$_3$O$_4$, AgNPs-Fe$_3$O$_4$, P(ABA)-Fe$_3$O$_4$ and AgNPs-P(ABA)-Fe$_3$O$_4$. The mass saturation magnetization (M$_s$) of Fe$_3$O$_4$ was 8.5 emu g^{-1}, indicating that it was superparamagnetic at room temperature. Compared to the Fe$_3$O$_4$, the magnetization of the modified magnetic iron oxide decreased significantly after being coated with of AgNPs, P(ABA) and AgNPs-P(ABA). The M$_s$ values of AgNPs-Fe$_3$O$_4$, P(ABA)-Fe$_3$O$_4$ and AgNPs-P(ABA)-Fe$_3$O$_4$ were 4.9, 3.0 and 2.4 emu g^{-1}, respectively; lower than the saturation magnetization of starting Fe$_3$O$_4$ material. The reason for the decrease of the saturation magnetization per weight was due to the surface modification of a magnetic support with non-magnetic shell structures. Moreover, coating of P(ABA) and AgNPs layers over Fe$_3$O$_4$ could efficiently shield the magnetite surface from
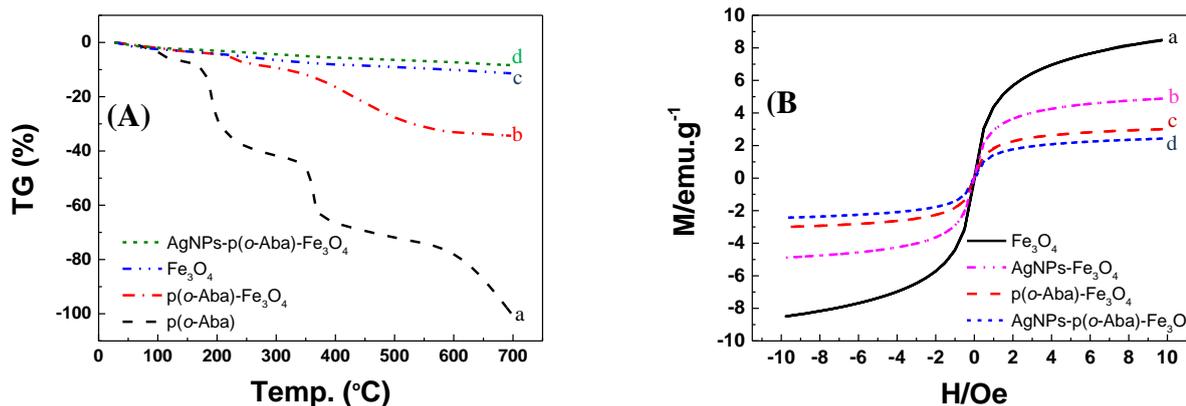
air contact.

Figure 4. (A) TGA curves of (a) P(ABA) (– –), (b) P(ABA)-Fe$_3$O$_4$ (·–), (c) Fe$_3$O$_4$ (–··), and (d) AgNPs-P(ABA)-Fe$_3$O$_4$ (········). (B) Hysteresis loops of (a) Fe$_3$O$_4$ (——), (b) AgNPs-Fe$_3$O$_4$ (–··), (c) P(ABA)-Fe$_3$O$_4$ (– –),and (d) AgNPs-P(ABA)-Fe$_3$O$_4$ (········).

3.3 Electrochemical sensing of H$_2$O$_2$

The electrochemical sensing of H$_2$O$_2$ was first tested for the response using cyclic voltammetry. Figure 5 shows the electrochemical behaviours of Fe$_3$O$_4$/MCPE, P(ABA)-Fe$_3$O$_4$/MCPE, AgNPs-Fe$_3$O$_4$/MCPE and AgNPs-P(ABA)-Fe$_3$O$_4$/MCPE in a 0.1 M N$_2$-saturated phosphate buffer (pH 7.5) with the absence of H$_2$O$_2$ and 4 mM H$_2$O$_2$ by the cyclic voltammograms (CVs) at a scan rate of 50 mV s^{-1}. The direction of the initial scan started at 0 V and went to the negative direction, and then was revered at -0.6 V. It was found that low and stable background currents were observed for all modified electrodes. Compared to the background current, the reduction peak current increased with addition of H$_2$O$_2$. The Fe$_3$O$_4$/MCPE showed a very low current response for to H$_2$O$_2$ sensing. The conducting polyanilines could enhance the electrical conductivity of composites, so we had modified the surface of Fe$_3$O$_4$ with P(ABA) via carboxylic acid functional groups [30, 31]. The current response of P(ABA)-Fe$_3$O$_4$/MCPE immediately increased with the presence of H$_2$O$_2$. As known, AgNPs played an important role in electrocatalytic performance of electrode, so the reduction of Ag$^+$ ions to AgNPs was achived upon the addition of NaBH$_4$ under sonication. The current response of AgNPs-Fe$_3$O$_4$ modified MCPE significantly increased and higher than the P(ABA)-Fe$_3$O$_4$/MCPE. It has also been reported that AgNPs could be easily adsorbed onto the carboxylated materials [32, 33]. So, the AgNPs-P(ABA)-Fe$_3$O$_4$ was prepared through the surface functionalization of Fe$_3$O$_4$ with P(ABA) and following the reduction of Ag$^+$ ions under sonication. Compared to Fe$_3$O$_4$/MCPE, P(ABA)-Fe$_3$O$_4$/MCPE and AgNPs-Fe$_3$O$_4$/MCPE, the AgNPs-P(ABA)-Fe$_3$O$_4$/MCPE exhibited the maximum current response towards the H$_2$O$_2$ reduction. This remarkable activity was attributed to the synergistic electrocatalytic effect of AgNPs, P(ABA) and Fe$_3$O$_4$ for electrochemical reduction of H$_2$O$_2$ [6, 43]. Thus, the AgNPs-P(ABA)-Fe$_3$O$_4$/MCPE was chosen for further investigations of other parameters for H$_2$O$_2$ sensing.
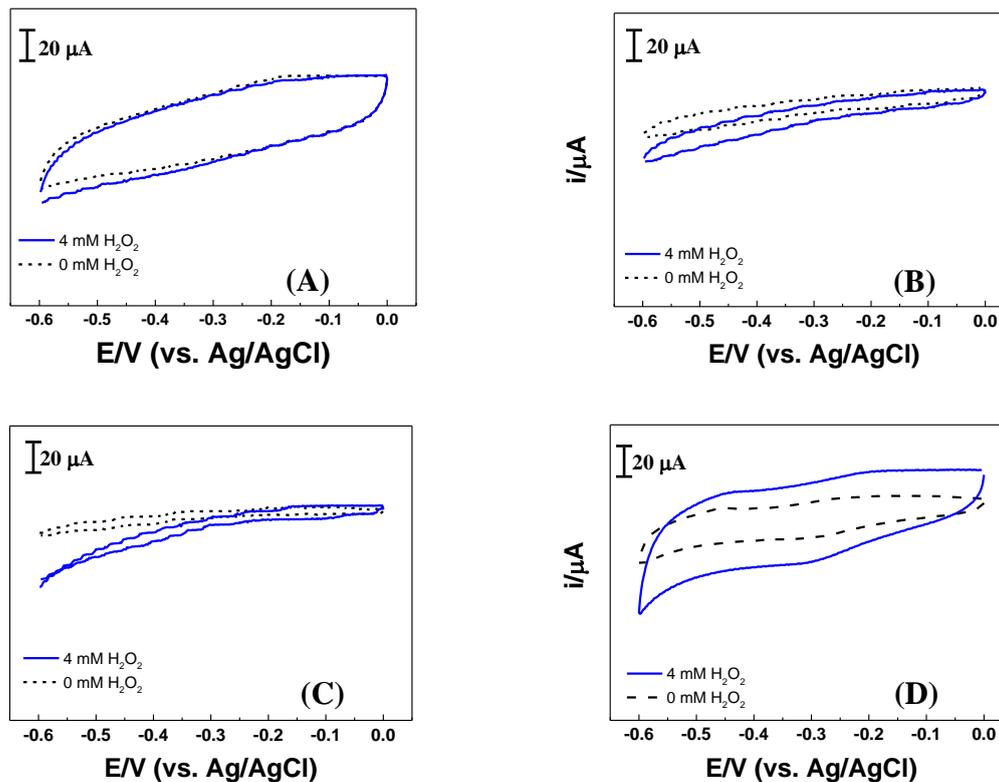
Figure 5. CVs of (A) Fe_3O_4/MCPE, (B) P(ABA)-Fe_3O_4/MCPE, (C) AgNPs-Fe_3O_4/MCPE and (D) AgNPs-P(ABA)-Fe_3O_4/MCPE in a 0.1 M N_2-saturated phosphate buffer (pH 7.5) with the absence of H_2O_2 (·········) and 4 mM H_2O_2 (——) at a scan rate of 50 mV/s.

According to previous literature reports [44-46], the electrocatalytic reduction of H_2O_2 in this study is expressed as follows:

$$2H_2O_2 \rightarrow O_2 + H_2O$$

H_2O_2 was decomposed into O_2 and H_2O catalyzed by the supported AgNPs. The generated oxygen was adsorbed the electrode surface in order to the formation of Ag_2O, which was reduced to Ag during the reverse scan [47].

3.4 Scan rate study

Figure 6A shows the CVs of 2 mM H_2O_2 at the AgNPs-P(ABA)-Fe_3O_4/MCPE with scan rate ranging from 20 to 250 mV s^{-1} (internal to external). It was found that the cathodic current was linearly proportional to $v^{1/2}$ in the range of 20-250 mV s^{-1}, indicating that this process was diffusion-controlled (see the inset of Figure 6A). The linear regression equation for the cathodic current was $y = -6.0177x + 28.0520$ with a linear correlation coefficient (r^2) of 0.9953.

3.5 Loading solution of AgNPs-P(ABA)-Fe₃O₄ composite

The loading solution of AgNPs-P(ABA)-Fe_3O_4 composite directly affects the sensitivity of the electrocatalytic reduction of H_2O_2. As shown in Figure 6B, effect of volume on electrochemical sensing towards 2 mM H_2O_2 was also investigated in a 0.1 M N_2-saturated phosphate buffer by varying the volume from 10 to 50 μL. The signal current increased to -46.4 μA when increasing the loading solution to 20 μL, and also no significant change was observed upon when increasing to 50 μL. As seen, the higher loading solutions resulted in the high thickness of the modified electrode. The results here are similar to findings reported by Qu *et al.*[37] who suggested that an excess composite could disturb the electron transfer on the electrode surface. Thus, the suitable loading solution of 20 μL was selected for the fabrication of AgNPs-P(ABA)-Fe_3O_4/MCPE.
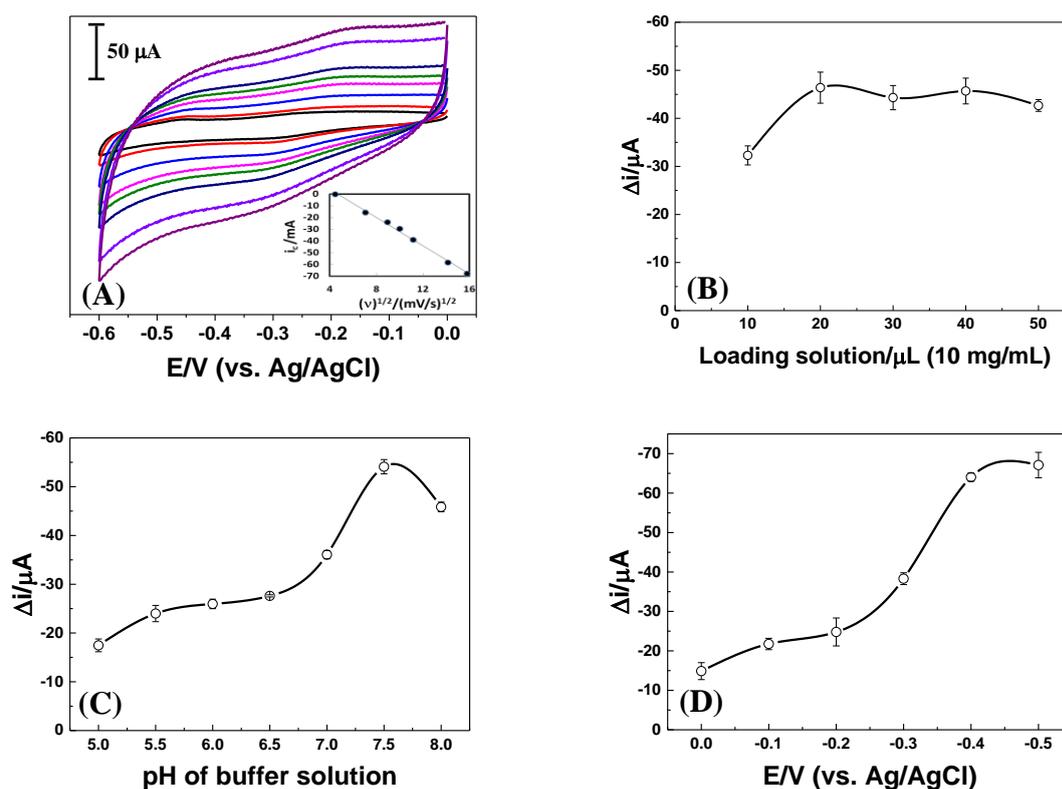

Figure 6. (A) CVs of 2 mM H_2O_2 at AgNPs-P(ABA)-Fe_3O_4/MCPE in 0.1 M N_2-saturated phosphate buffer (pH 7.5) with scan rate ranging from 20 to 250 mV/s (internal to external). The inset (A) shows the plot of the cathodic current (i_c) versus $v^{1/2}$. (B) Effect of loading solution, (C) Effect of pH of buffer solution, and (D) Effect of applied potential on the reduction current on the AgNPs-P(ABA)-Fe_3O_4/MCPE towards electrochemical sensing of 2 mM H_2O_2 in 0.1 M N_2-saturated phosphate buffer.

3.6 pH of buffer solution

The effect of pH (from pH 5.0 to 8.0) of buffer solution towards electrochemical sensing of 2 mM H_2O_2 was investigated in a 0.1 M N_2-saturated phosphate buffer with an applied potential of -0.4

V. As shown in Figure 6C, the signal current from the electrocatalytic reduction of H_2O_2 at AgNPs-P(ABA)-Fe_3O_4/MCPE was relatively small in an acidic medium, which was attributed to the instability of metallic silver in an acidic solution. After that, the signal current rapidly increased from pH 5.0 to 7.5, and then decreased again when pH dropped from pH 7.5 to 8.0. Thus, to obtain the maximum activity, pH 7.5 was chosen as the buffer solution for electroanalytical determination of H_2O_2.

3.7 Applied potential

The effect of applied potential on the electrochemical sensing towards H_2O_2 was carried out in a 0.1 M N_2-saturated phosphate buffer (pH 7.5). As shown in Figure 6D, it was found that the cathodic current (i_c) from electrochemical sensing of 2 mM H_2O_2 tended to increase when the applied potential was changed from 0 to -0.5 V. A small signal current was observed when applying the potential below -0.2 V. The signal current dramatically increased at the applied potential of -0.4 V, and then was stable at -0.5 V. Thus, the suitable applied potential of -0.4 V versus Ag/AgCl (sat. 3.0 M KCl) was selected for the determination of H_2O_2 in this work.
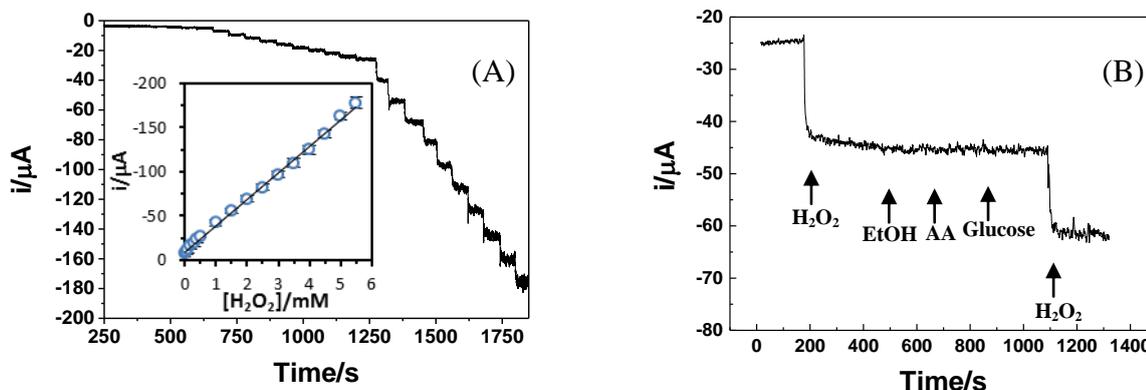
3.8 Amperometric sensing towards H_2O_2

Figure 7. (A) Amperometric responses of AgNPs-P(ABA)-Fe_3O_4/MCPE with the successive injections of H_2O_2 in a stirring 0.1 M N_2-saturated phosphate buffer (pH 7.5) at an applied potential of -0.4 V. Inset (A) shows a calibration plot for H_2O_2. (B) An amperometric response of AgNPs-P(ABA)-Fe_3O_4/MCPE to the successive addition of 1 mM H_2O_2, 2 mM ethanol (EtOH), 2 mM ascorbic acid (AA), 2 mM glucose, and 1 mM H_2O_2, respectively.

The electrocatalytic activity of AgNPs-P(ABA)-Fe_3O_4/MCPE towards H_2O_2 electro-reduction was investigated using amperometry. As shown in Figure 7A, the fabricated sensor exhibited a high stepped growth of reduction currents and fast response time within 5 s under the optimum condition. The inset in Figure 7A shows a calibration plot towards electrochemical sensing of H_2O_2 obtained at AgNPs-P(ABA)-Fe_3O_4/MCPE. The linear range was observed in a wide range of 5 μM to 5.5 mM. The linear regression equation was $i(\mu A) = -2.97C(\mu M) - 1.042$, where C is the H_2O_2 concentration in

the bulk solution with correlation coefficient (r^2) of 0.9978. The limit of detection (LOD) was 1.74 μM, based on a signal-to-noise (S/N) ratio of 3. Table 1 shows the comparison of the developed electrode system with the recently reported electrode systems towards the sensing of H_2O_2. It was found that the analytical characteristic of the developed sensor was better than the previous ones reported for the H_2O_2 sensors with regard to the detection limit and linear concentration range.

Table 1. Comparison of the developed electrode system with the recently reported electrode systems towards the sensing of H_2O_2.

Electrode system	Supporting solution (pH)	Potential (V)	Linear range (mM)	LOD (μM)	Reference
PEI-AgNCs/GCE	PBS (pH 7.0)	-0.78	0.01-1.44	1.80	[43]
Ag-MnO$_2$-MWCNTs/GCE	PBS (pH 7.2)	-0.30	0.005-10.4	1.70	[46]
AgNP/ZnO/GCE	PBS (pH 7.4)	-0.25	0.002-5.5	0.42	[48]
Ag microsphere/GCE	PBS (pH 7.0)	-0.50	0.2-2.0	1.20	[49]
AgNPs-p(Ay R)/GCE	PBS (pH 6.0)	-0.40	0.001-0.45	0.32	[50]
DNA-AgNCs/Graphene/GCE	PBS (pH 7.0)	-0.70	0.015-23	3.0	[51]
(PDDA-Graphene/Fe$_3$O$_4$)$_n$/ITO	PBS (pH 7.0)	-0.40	0.02-6.25	2.5	[52]
AgNPs-P(ABA)-Fe$_3$O$_4$/MCPE	PBS (pH 7.5)	-0.40	0.005-5.5	1.74	This work

PEI = Polyethyleneimine, AgNCs = Silver nanoclusters, MWCNTs = Multiwall carbon nanotubes, p(Ay R) = poly(alizarin yellow R), PDDA = Poly(diallydimethylammonium chloride), GCE = Glassy carbon electrode, ITO = Indium tin oxide

3.9 Reproducibility and stability of the AgNPs-P(ABA)-Fe$_3$O$_4$/MCPE

In order to study the reproducibility, five nonenzymatic sensors using a carbon paste electrode modified with AgNPs-P(ABA)-Fe$_3$O$_4$ were fabricated by the same method (see Section 2.4), and were used to test 1 mM H_2O_2 under the optimum condition. It was found that the coefficients of variation for inter-assay were 3.4%, indicating a good reproducibility of the fabricated sensor. In addition, the operational stability of AgNPs-P(ABA)-Fe$_3$O$_4$/MCPE was investigated using amperometry every day for one week. It was found that the current response obtained from 1 mM H_2O_2 maintained 94% of original value on the 7th day of use. This indicated that the fabricated sensor possessed a good stability in practical.

3.10 Interference study and application in pharmaceutical products

The interference study was carried out using the developed nonenzymatic sensor in the presence of the common interfering species in the stirring 0.1 M N_2-saturated phosphate buffer (pH 7.5) at an applied potential of -0.4 V. Figure 7B shows an amperometric response of AgNPs-P(ABA)-Fe$_3$O$_4$/MCPE to the successive addition of 1 mM H_2O_2, 2 mM ethanol (EtOH), 2 mM ascorbic acid

(AA), 2 mM glucose, and 1 mM H_2O_2, respectively. It was found that the AgNPs-P(ABA)-Fe_3O_4/MCPE was highly selective to H_2O_2 detection. The developed sensor displayed remarkable tolerance to interfering substances. The selected substances did not interfere significantly with the determination of H_2O_2, although the concentration of the interfering substances was as 2 times greater than that of H_2O_2. This may be due to the low working potential of -0.4 V, meaning no electrochemical reactions occurred at this potential. Thus, the selective and sensitive determination of H_2O_2 was achieved using AgNPs-P(ABA)-Fe_3O_4/MCPE.

In order to verify the applicability of the developed sensor, the H_2O_2 concentration in real samples was investigated. Two pharmaceutical products of disinfectant solutions containing H_2O_2 were determined using our developed sensor. The selected samples were diluted to an appropriate level with a phosphate buffer prior to electroanalysis. Table 2 shows the analytical application of AgNPs-P(ABA)-Fe_3O_4/MCPE for the determination of H_2O_2 in real samples compared with the titrimetric $KMnO_4$ method. A recovery study was also performed on the two samples. The results showed that the determined amounts of H_2O_2 in real samples were in good agreement with the values obtained from the $KMnO_4$ titrimetric method. In addition, the %recovery and %RSD were also acceptable values, indicating that the developed sensor was feasible for the determination of H_2O_2 in the real samples.

Table 2. Analytical application of AgNPs-P(ABA)-Fe_3O_4/MCPE for the determination of H_2O_2 in real samples compared with the titrimetric $KMnO_4$ method (n = 3).

Sample No.	Sample (mM)	AgNPs-P(ABA)-Fe_3O_4/MCPE				Titrimetric $KMnO_4$ method			
		Added (mM)	Found (mM)	Recovery (%)	RSD (%)	Added (mM)	Found (mM)	Recovery (%)	RSD (%)
1	0.5	-	0.49 ± 0.02	99.63	3.05	-	0.51 ± 0.01	103.25	2.40
		0.1	0.61 ± 0.01	102.04	2.80	0.1	0.61 ± 0.02	102.04	2.02
		0.4	0.88 ± 0.05	98.21	5.12	0.4	0.90 ± 0.01	100.14	1.40
2	0.5	-	0.50 ± 0.02	100.52	4.20	-	0.51 ± 0.01	102.37	2.09
		0.1	0.60 ± 0.02	100.15	3.84	0.1	0.61 ± 0.01	102.08	2.02
		0.4	0.92 ± 0.05	103.23	4.83	0.4	0.91 ± 0.01	100.62	1.18

4. CONCLUSION

A composite consisting of AgNPs, P(ABA) and Fe_3O_4 was prepared under sonication and then characterized using transmission electron microscopy (TEM), thermogravimetric analysis (TGA), and vibrating sample magnetometer (VSM). A nonenzymatic sensor for H_2O_2 was fabricated by casting AgNPs-P(ABA)-Fe_3O_4 composite onto the surface of a magnetic carbon paste electrode (MCPE). The

electrochemical investigations indicated that the AgNPs-P(ABA)-Fe$_3$O$_4$/MCPE showed an excellent response current of H$_2$O$_2$ reduction, compared with the Fe$_3$O$_4$, P(ABA)-Fe$_3$O$_4$ and AgNPs-Fe$_3$O$_4$. Under the optimum condition, the calibration curve for H$_2$O$_2$ was obtained in a wide range of 5 µM to 5.5 mM with the LOD of 1.74 µM (S/N = 3). The AgNPs-P(ABA)-Fe$_3$O$_4$/MCPE provided a cheap, highly selective and sensitive amperometric approach for H$_2$O$_2$ sensing in a variety of fields such as pharmaceutical, clinical, environmental and industrial applications.

References

1. S. Neill, R. Desikan, J. Hancock, *Curr. Opin. Plant Biol.* 5 (2002) 388.
2. C. E. Huckaba, F. G. Keyes, *J. Am. Chem. Soc.* 70 (1948) 1640.
3. A. C. Pappas, C. D. Stalikas, Y. C. Fiamegos, M. I. Karayannis, *Anal. Chim. Acta* 455 (2002) 305.
4. A.-L. Hu, Y.-H. Liu, H.-H. Deng, G.-L. Hong, A.-L. Liu, X.-H. Lin, X.-H. Xia, W. Chen, *Biosens Bioelectron.* 61 (2014) 374.
5. K. A. Fähnrich, M. Pravda, G. G. Guilbault, *Talanta* 54 (2001) 531.
6. Y. Li, Q. Lu, S. Wu, L. Wang, X. Shi, *Biosens Bioelectron.* 41 (2013) 576.
7. X. Li, X. Liu, W. Wang, L. Li, X. Lu, *Biosens Bioelectron.* 59 (2014) 221.
8. S. Chairam, P. Buddhalee, M. Amatatongchai, *Int. J. Electrochem. Sci.* 8 (2013) 10250.
9. R. N. Adams, *Anal. Chem.* 30 (1958) 1576.
10. D. Bellido-Milla, L. Cubillana-Aguilera, M. El Kaoutit, M. Hernández-Artiga, J. Hidalgo-Hidalgo de Cisneros, I. Naranjo-Rodríguez, J. Palacios-Santander, *Anal Bioanal Chem* 405 (2013) 3525.
11. I. Švancara, A. Walcarius, K. Kalcher, K. Vytřas, *Cent.Eur. J. Chem.* 7 (2009) 598.
12. T. Ruzgas, E. Csöregi, J. Emnéus, L. Gorton, G. Marko-Varga, *Anal. Chim. Acta* 330 (1996) 123.
13. B. Dinesh, V. Mani, R. Saraswathi, S.-M. Chen, *RSC Advances* 4 (2014) 28229.
14. K.-J. Huang, D.-J. Niu, X. Liu, Z.-W. Wu, Y. Fan, Y.-F. Chang, Y.-Y. Wu, *Electrochim. Acta* 56 (2011) 2947.
15. A. T. Ezhil Vilian, S.-M. Chen, B.-S. Lou, *Biosens Bioelectron.* 61 (2014) 639.
16. S. Palanisamy, C. Karuppiah, S.-M. Chen, R. Emmanuel, P. Muthukrishnan, P. Prakash, *Sens. Actuators, B* 202 (2014) 177.
17. V. Mani, B. Dinesh, S.-M. Chen, R. Saraswathi, *Biosens Bioelectron.* 53 (2014) 420.
18. W. Tao, D. Pan, Y. Liu, L. Nie, S. Yao, *Anal. Biochem.* 338 (2005) 332.
19. S. Kango, S. Kalia, A. Celli, J. Njuguna, Y. Habibi, R. Kumar, *Prog. Polym. Sci.* 38 (2013) 1232.
20. X. Chen, G. Wu, Z. Cai, M. Oyama, X. Chen, *Microchim Acta* 181 (2014) 689.
21. A. Ravindran, P. Chandran, S. S. Khan, *Colloids Surf., B* 105 (2013) 342.
22. S. Chen, R. Yuan, Y. Chai, F. Hu, *Microchim Acta* 180 (2013) 15.
23. J. D. Stenger-Smith, *Prog. Polym. Sci.* 23 (1998) 57.
24. E. T. Kang, K. G. Neoh, K. L. Tan, *Prog. Polym. Sci.* 23 (1998) 277.
25. M. Jaymand, *Prog. Polym. Sci.* 38 (2013) 1287.
26. G. Ćirić-Marjanović, *Synth. Met.* 170 (2013) 31.
27. R. Hao, R. Xing, Z. Xu, Y. Hou, S. Gao, S. Sun, *Adv. Mater.* 22 (2010) 2729.

28. C. G. C. M. Netto, H. E. Toma, L. H. Andrade, *J. Mol. Catal. B: Enzym.* 85–86 (2013) 71.
29. M. Zhu, G. Diao, *Nanoscale* 3 (2011) 2748.
30. T. Alizadeh, *Biosens Bioelectron.* 61 (2014) 532.
31. C. Boyer, M. R. Whittaker, V. Bulmus, J. Liu, T. P. Davis, *NPG Asia Mater* 2 (2010) 23.
32. D. Jiang, Y. Zhang, M. Huang, J. Liu, J. Wan, H. Chu, M. Chen, *J. Electroanal. Chem.* 728 (2014) 26.
33. A. A. Abdelwahab, Y.-B. Shim, *Sens. Actuators, B* 201 (2014) 51.
34. H. S. O. Chan, S. C. Ng, W. S. Sim, K. L. Tan, B. T. G. Tan, *Macromolecules* 25 (1992) 6029.
35. U. Schwertmann, R. M. Cornell, Iron oxides in the laboratory: Preparation and characterization, Wiley-VCH, Weinheim, 1991, p. 111.
36. J.-D. Qiu, M. Xiong, R.-P. Liang, H.-P. Peng, F. Liu, *Biosens Bioelectron.* 24 (2009) 2649.
37. S. Qu, J. Wang, J. Kong, P. Yang, G. Chen, *Talanta* 71 (2007) 1096.
38. H. Xu, K. S. Suslick, *ACS Nano* 4 (2010) 3209.
39. H. Xu, B. W. Zeiger, K. S. Suslick, *Chem. Soc. Rev.* 42 (2013) 2555.
40. J. K. Oh, J. M. Park, *Prog. Polym. Sci.* 36 (2011) 168.
41. Y. Lin, L. Li, L. Hu, K. Liu, Y. Xu, *Sens. Actuators, B* 202 (2014) 527.
42. P. Swapna Rao, D. N. Sathyanarayana, *Polymer* 43 (2002) 5051.
43. B. L. Li, J. R. Chen, H. Q. Luo, N. B. Li, *J. Electroanal. Chem.* 706 (2013) 64.
44. M. Honda, T. Kodera, H. Kita, *Electrochim. Acta* 31 (1986) 377.
45. W. Bai, J. Zheng, Q. Sheng, *Electroanal.* 25 (2013) 2305.
46. Y. Han, J. Zheng, S. Dong, *Electrochim. Acta* 90 (2013) 35.
47. Q. Yi, F. Niu, L. Li, R. Du, Z. Zhou, X. Liu, *J. Electroanal. Chem.* 654 (2011) 60.
48. Q. Wang, J. Zheng, *Microchim Acta* 169 (2010) 361.
49. B. Zhao, Z. Liu, Z. Liu, G. Liu, Z. Li, J. Wang, X. Dong, *Electrochem. Commun.* 11 (2009) 1707.
50. K. Zhang, N. Zhang, L. Zhang, J. Xu, H. Wang, C. Wang, T. Geng, *Microchim Acta* 173 (2011) 135.
51. Y. Xia, W. Li, M. Wang, Z. Nie, C. Deng, S. Yao, *Talanta* 107 (2013) 55.
52. X. Liu, H. Zhu, X. Yang, *Talanta* 87 (2011) 243.